RSC Advances

PAPER

Cite this: *RSC Adv.*, 2016, **6**, 96490

Photovoltaically self-charging cells with $WO_3 \cdot H_2O$/CNTs/PVDF composite†

Xuezhen Huang,‡[a] Xi Zhang‡[a] and Hongrui Jiang*[ab]

Two-electrode photovoltaically self-charging cells (PSCs) possess compact structures for both energy conversion and storage with shared electrolyte and electrodes. It remains challenging to develop PSCs that are efficient in both energy conversion and storage. In this work, $WO_3 \cdot H_2O$ nanoplates were synthesized by a modified acid-directed hydrothermal process and used to prepare a $WO_3 \cdot H_2O$/CNTs/PVDF composite film for energy storage in PSCs. The method with the assistance of polyethylenimine was essential to form smaller sized $WO_3 \cdot H_2O$ nanoplates, thus larger surface area and higher columbic efficiency in cyclic voltammetry tests. Such an electrode composite made it more facile to assemble PSCs, which displayed an energy conversion efficiency of 2.12% with simultaneous energy storage of 1.38 C cm^{-2}. Higher Li^+ concentration in the electrolyte will be helpful to maintain the photocurrent at a larger value during irradiation. A higher performance of PSCs can be potentially obtained by optimizing the contact of electron collector and pseudocapacitive electrode materials.

Received 24th August 2016
Accepted 4th October 2016

DOI: 10.1039/c6ra21303k

www.rsc.org/advances

1. Introduction

Photovoltaically self-charging cells (PSCs) have been explored extensively with various integration strategies; they combine energy conversion and storage into a single device to cope with the major drawback of solar power, *i.e.* dependence on the availability of sunlight.[1–11] The photon-to-electron conversion mechanism of dye-sensitized solar cells (DSSCs) provides a promising approach to the energy conversion side of the PSCs because of their high light-to-electricity conversion efficiency (η) and low cost. It is thus interesting to study if the sandwiched structure and electrochemical system of DSSCs can be shared with an energy storage system, *e.g.* supercapacitor, to form a hybrid and compact PSC device, particularly a two-electrode PSC. To date, few studies have been done with two-electrode PSCs. Takshi *et al.* demonstrated a two-electrode PSC with a polymers/dye-activated carbon electrode system and showed an open-circuit voltage (V_{oc}) of 0.43 V and a capacitance of 1.04 mF.[12] Our previous work[13,14] exhibited that DSSCs with polyvinylidene fluoride (PVDF) dielectric composites on the counter electrodes could realize dual functions of energy conversion and storage with a charging voltage of 0.75 V.

The structure of our previous PSCs utilized Au/Pt layer as a quasi-electrode to realize the cycle of I^-/I_3^- redox reaction, and the counter electrode was kept from contacting Li-ion-containing electrolyte by a layer of PVDF dielectric film.[13] In other words, the energy storage mechanism was electrical double layer and the electrolyte was not shared between the energy conversion and storage parts. The limited surface area of PVDF film therefore hinders the increase of capacitance of the PSCs. In this work, we have developed a two-electrode PSC, where the porous energy storage part allows for the penetration of the Li ion containing electrolyte. Meanwhile, it provides an interface for the reduction of I_3^- to I^- without the presence of the quasi-electrode. More importantly, such design affords more room to improve the capacitance of PSCs by applying new materials for energy storage.

Nanostructured metal oxides such as tungsten oxide (WO_3) with several oxidation states are especially useful for energy storage owing to their pseudocapacitance.[15,16] WO_3 is an n-type semiconducting oxide that has high electronic conductivity (10 to 10^{-6} s cm^{-1}), high intrinsic density (>7 g cm^{-3}) and superior electrochemical performance.[17–21] Specifically, WO_3 has high pseudocapacitance, resulting from electrochemical intercalation/deintercalation with protons following the application of a low voltage. However, our experiments indicated that nanostructured WO_3 directly grown on fluorine-containing tin oxide (FTO) substrates did not work well with PVDF on the counter electrode for both energy conversion and storage, owing to its poor electrical conductivity. Hierarchically nanostructured WO_3 has been used to form freestanding flexible composite with carbon nanotubes (CNTs) and PVDF for high performance all-solid-state flexible micro-pseudocapacitor.[16] However, CNTs could not access the

[a]*Department of Electrical and Computer Engineering, University of Wisconsin-Madison, 1415 Engineering Drive, Madison, Wisconsin 53706, USA. E-mail: hongrui@engr.wisc.edu*

[b]*Department of Materials Science and Engineering, University of Wisconsin-Madison, 1509 University Avenue, Madison, Wisconsin 53706, USA*

† Electronic supplementary information (ESI) available. See DOI: 10.1039/c6ra21303k

‡ Xuezhen Huang and Xi Zhang contributed to the work equally.

interior space of the hierarchical structure of WO_3 to establish good contact for carrier diffusion, thus resulting in relatively low faradic efficiency. To improve the contact between electroconductive and pseudocapacitive materials, $WO_3 \cdot H_2O$ nanoplates were fabricated for energy storage applications with the assistance of polyethylenimine (PEI).[22–25] The modified synthesis kept WO_3 from forming hierarchical structures, but instead produced smaller-sized nanoplates, hence larger surface area.

In this work, we combined the modified $WO_3 \cdot H_2O$ nanoplates with CNTs/PVDF to realize a composite film, and applied it to the counter electrodes of PSCs as the energy storage part. This composite considerably enhanced the columbic efficiency of the electrode. The formed PSC had a η of 2.12%, and achieved concurrent energy storage with a charge density of 1.38 C cm^{-2}. This work has potential applications in low-power consumption devices and electronics as continuous and unattended power supply.

2. Experimental

2.1. Synthesis of WO_3 nanostructures

In a typical experiment, 100 mL Na_2WO_4 (0.08 M) solution, 100 mL citric acid (0.10 M) and 1 drop of branched PEI (low molecular weight) were added into a glass container, followed by adding HCl (5 M) to the container to adjust the pH value to 0.5, monitored by a pH tester (Oakton, EW-35634-30). The container covered by a glass slide was subsequently placed in a furnace maintained at 90 °C for 4 h. The final reactive solution was clear and the yellow $WO_3 \cdot H_2O$ precipitate was found on the bottom and side wall of the reactor. This precipitate was washed with DI water and centrifuged three times to remove impurities. The $WO_3 \cdot H_2O$ powder was dried in air at 100 °C for 12 h. All chemicals were purchased from Sigma-Aldrich.

2.2. Electrode paste preparation

Nanostructured $WO_3 \cdot H_2O$ (1 g) was ground with PVDF (0.5 g) (Kynar 301F, $M_w = 3.8 \times 10^5$) and CNTs (0.5 g) (Sigma-Aldrich, O.D. × *L* 6–9 nm × 5 μm, >95%), and then *N*-methyl-2-pyrrolidone (20 mL) was added in the mixture to form a paste by stirring and sonication for 1 h, respectively. The paste was cast onto a glass slide to prepare the electrode films as described in ref. 16. The thickness of films were measured with a Mitutoyo ID-C112E digimatic indicator.

2.3. PSC fabrication

Photoelectrode of PSCs were prepared by doctor-blade coating of a TiO_2-containing viscous paste (Solaronix, 15–20 nm particles, Switzerland) onto the FTO substrate, followed by sintering at 500 °C for 1 h. The films (~120 °C) were then immersed into a 0.3 mM solution of ruthenium complex N719 dye (Solaronix, Aubonne, Switzerland) in dry ethanol for 24 h. The counter electrode of PSCs were prepared by physically attaching the $WO_3 \cdot H_2O$/CNTs/PVDF composite film (5 mm × 5 mm) onto the FTO glass. Then, a Pt layer was deposited onto the counter electrode by a 2 min electrodeposition process in chloroplatinic acid (Aldrich, USA) solution (0.5 M), followed by a drying process at 100 °C under vacuum. TiO_2 photoelectrode and counter electrode were assembled together by a 100 μm spacer (Surlyn, Solaronix, Switzerland). The internal space of the cell was filled with a liquid electrolyte [0.05 M LiI, 0.03 M I_2, 0.1 M guanidinium thiocyanate (GNCS), 1.0 M 1,3-dimethylimidazolium iodide (DMII), 0.5 M 4-*tert*-butyl pyridine (TBP) in 3-methoxypropionitrile and acetonitrile (6 : 4)].

2.4. Instrumentation

The morphology of $WO_3 \cdot H_2O$/CNTs/PVDF composite was characterized by an SEM (Zeiss LEO 1530 containing a detector with a resolution of 129 eV at manganese and a light element detection limit of boron). The XRD spectrum of PVDF film was measured by a Bruker/Siemens Hi-Star 2d X-ray diffractometer with a monochromatic Cu K-alpha point source (0.8 mm). The photocurrent density–voltage (*J*–*V*) performance was tested using a Keithley 2400 source meter under AM 1.5G simulated sunlight (Newport 94022A equipped with a 150 W Xe lamp and AM 1.5G filter). The photovoltage and photocurrent transient curves (*V*–*t*, *J*–*t*) measurements were carried out by an Agilent 34411A $6_{1/2}$ digital multimeter. $WO_3 \cdot H_2O$/CNTs/PVDF electrodes and PSCs were characterized by cyclic voltammetry (CV) and electrochemical impedance spectroscopy using a BAS 100B Electrochemical Analyzer. The CV of electrodes was measured in a three-electrode system (*vs.* an Ag/AgCl reference electrode). A platinum foil was placed 1 cm away from the electrodes as the counter electrode.

3. Results and discussion

3.1. Preparation and characterization of $WO_3 \cdot H_2O$ nanoplates

The square $WO_3 \cdot H_2O$ nanoplates was prepared by heating the mixed solution of Na_2WO_4 (0.125 M) and citric acid (0.125 M) with 1 : 1 ratio at 90 °C following a procedure described in ref. 16. These nanoplates usually have a dimension of 400 × 400 × 50 nm^3. With reduced pH values and concentrations of reactants, the size of nanoplates could be decreased; yet, spherical hierarchical structures could form *via* secondary growth as we reported before.[16] PEI is a popular stabilizer, which can be used to protect nanostructures from agglomeration and inhibit crystallite-size growth of nanomaterials.[22,23] Fig. 1 shows $WO_3 \cdot H_2O$ nanoplates fabricated with PEI assistance and morphologies of $WO_3 \cdot H_2O$/CNTs/PVDF composite film. The size of nanoplates went down to 150 × 150 × 25 nm^3 without cross growth leading to hierarchical structures, which were conducive to high performance supercapacitors.[24,25] XRD spectra (Fig. 2) reveals that only the spectrum of $WO_3 \cdot H_2O$ could be observed with preferential growth in the (111) direction (ICDD PDF 00-043-0679). Compared with the XRD spectrum of tungsten oxide nanoplates prepared without PEI, the crystal growth along (020) at the peak of 16.53 degree was restrained remarkably, which probably contributed to the elimination of two nanoplates growing together and intersecting each other at 45 degree as shown in ref. 16. TEM images in

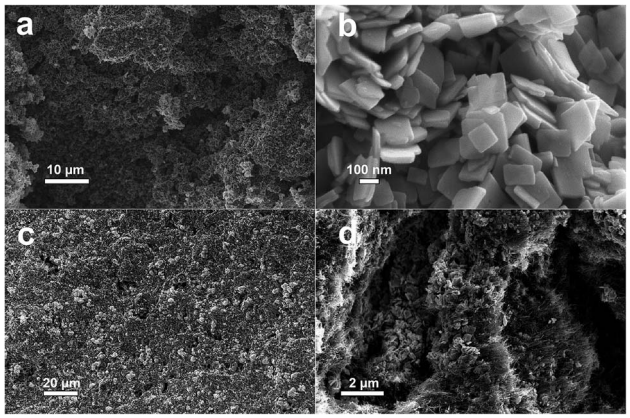

Fig. 1 (a) SEM images of $WO_3 \cdot H_2O$ nanoplates and (b) in large magnification. (c) The surface morphology of $WO_3 \cdot H_2O$/CNTs/PVDF (50 : 25 : 25) film and (d) its cross-section.

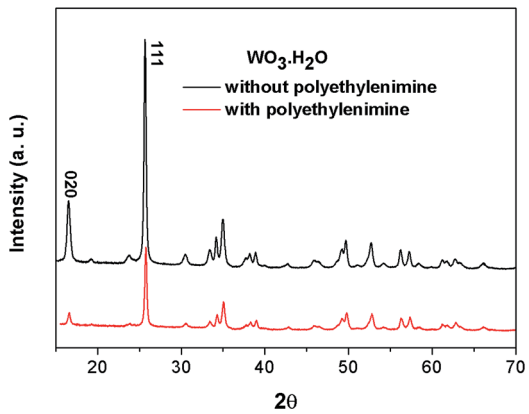

Fig. 2 XRD spectra of tungsten oxide nanoplates.

Fig. 3 show more detail of the nanoplates and a preferential growth along the (111) direction.

3.2. Working mechanism

The morphology of $WO_3 \cdot H_2O$/CNTs/PVDF (50 : 25 : 25) film is shown in Fig. 1c, d and S1† shows its energy-dispersive X-ray spectroscopy (EDX). It was attached onto the counter

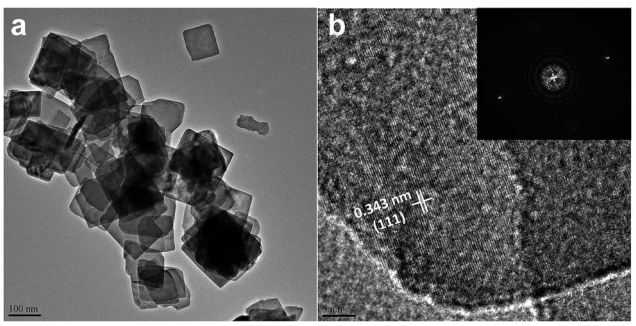

Fig. 3 TEM image (a) and HRTEM image (b) of $WO_3 \cdot H_2O$ nanoplates. Scale bars are 100 nm and 5 nm, respectively (inset, the fast-Fourier transform image).

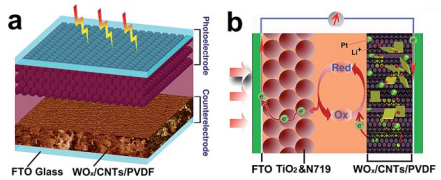

Fig. 4 Schematics of the structure and mechanism of TiO_2 DSSC with energy storage function by $WO_3 \cdot H_2O$/CNTs/PVDF composite film.

electrode to realize energy storage as shown in Fig. 4a. The majority of the photon-generated current passes through the FTO electrode surface to the interface between Pt/CNTs and the DSSC electrolyte for the photoelectric conversion; the rest of the charge accumulates on the surface of the $WO_3 \cdot H_2O$/CNTs/PVDF electrode and intercalates with Li^+, giving rise to energy storage as shown in Fig. 4b. All WO_3 hydrates are built from layers of corner-sharing octahedral units of $[WO_6]$ connected by hydrogen bridges of interlayer water molecules. These intercalated water molecules offer $WO_3 \cdot H_2O$ with enhanced intercalation properties towards cationic species compared with anhydrous WO_3.[26]

In this work, $WO_3 \cdot H_2O$ nanoplates were used to form two types of $WO_3 \cdot H_2O$/CNTs/PVDF flexible electrode films with 50 wt% and 60 wt%, respectively. Lower composition of WO_3 in the electrode has smaller capacitance as found in ref. 16. Fig. 5a shows the cyclic voltammetry (CV) curves of the electrode containing 50% of $WO_3 \cdot H_2O$ nanoplates at different scan rate from −0.2 to 0.8 V with a change of scan rate of 1–100 mV s^{-1}. The characteristic redox peaks of as-prepared electrode were observed. Accordingly, current became larger and peak potentials moved to higher voltage with increased scan rates, which was probably due to a finite time constant in the $WO_3 \cdot H_2O$/CNTs/PVDF electrodes.[27] Fig. 5b shows the specific capacitances of electrodes with different compositions. The electrode with 50% of $WO_3 \cdot H_2O$ nanoplates exhibited a maximum specific capacitance of 195 F cm^{-3} at a scan rate of 1 mV s^{-1}. When the composition of $WO_3 \cdot H_2O$ nanoplates was increased to 60%, the specific capacitance decreased to 50 F cm^{-3} owing to reduced amount of CNTs and lower electrical conductivity. As a comparison, the CV curve of the electrode containing 50% of hierarchical nest-like WO_3 nanostructure[16] is also shown in Fig. 5b. Its specific

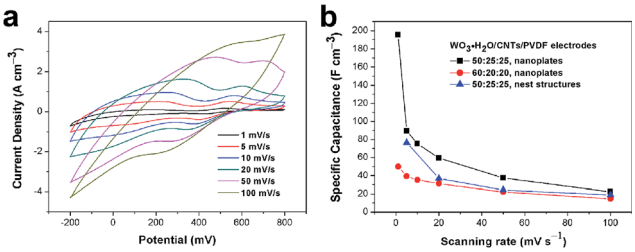

Fig. 5 (a) CV curves of $WO_3 \cdot H_2O$/CNTs/PVDF (50 : 25 : 25) electrodes at various scan rates in 2 M H_2SO_4 solution and (b) volumetric specific capacitance of three types of electrodes at different scan rates.

capacitance at a scan rate of 5 mV s^{-1} was up to 77 F cm^{-3}, higher than the one with 60% of $WO_3 \cdot H_2O$ nanoplates (39 F cm^{-3}) but lower than that with 50% $WO_3 \cdot H_2O$ nanoplates (89 F cm^{-3}). However, the decreasing percentage of specific capacitance from 5 to 20 mV s^{-1} of scan rate, 20% and 33% for electrodes with 60% and 50% of $WO_3 \cdot H_2O$, respectively, is much higher than the electrode with hierarchical WO_3 (52%). It indicates that the modified $WO_3 \cdot H_2O$/CNTs/PVDF electrodes have higher faradic efficiency, mainly because of better mixture of and contact between CNTs and $WO_3 \cdot H_2O$ nanoplates. The $WO_3 \cdot H_2O$/CNTs/PVDF composite with 50% WO_3 was used to build PSCs in this work.

3.3. Performance of PSCs

Here the $WO_3 \cdot H_2O$/CNTs/PVDF composite is porous and could not isolate the FTO substrate and the electrolyte. The electrochemical characterization showed that such pseudocapacitive materials realized the function of energy storage. Fig. 6 shows the η of PSCs under different working conditions. The PSC without Pt coating on the counter electrode displayed an efficiency of 1.44% and V_{oc} of 0.58 V, because multi-walled CNTs can be used as catalyst in counter electrode for I_3^- reduction in DSSCs.[28] Nonetheless, its efficiency was lower than both PSCs with Pt catalyst on the counter electrode. The highest η achieved was 2.12% with a V_{oc} of 0.62 V from the PSC with Pt catalyst on the counter electrode and 0.05 M LiI in the electrolyte. Li ion is known to improve the photocurrent of DSSCs while simultaneously reducing V_{oc}. Jennings *et al.* found that the addition of Li^+ to the electrolyte of DSSCs increased the electron injection efficiency across all wavelengths, thus leading to an increase in the photocurrent onset wavelength, and the electron diffusion length.[29] We observed that there was a dip in the *J*–*V* curve of PSCs in the range of 0–0.4 V. We believe that it resulted from the quick decrease of Li^+ concentration due to their accumulation on the counter electrode, which was not sufficient to support large photocurrent. Theoretically, Li ion would be consumed if the intercalation reaction happens between Li^+ and $WO_3 \cdot H_2O$. We then fabricated a PSC with saturated LiI in the electrolyte. Its *J*–*V* curve showed a flatter line shape in the range of 0–0.4 V. The PSC exhibited an efficiency of 1.88% and a V_{oc} of 0.55 V. The higher photocurrent and relatively lower photovoltage is consistent with the observation from a simple DSSC. The result implies that increased Li^+ concentration in the electrolyte of a PSC could be critical to the balance between energy conversion and storage.

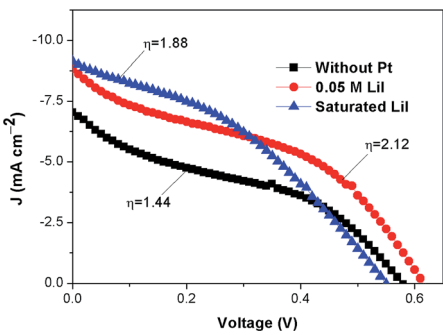

Fig. 6 *J*–*V* curves of PSCs.

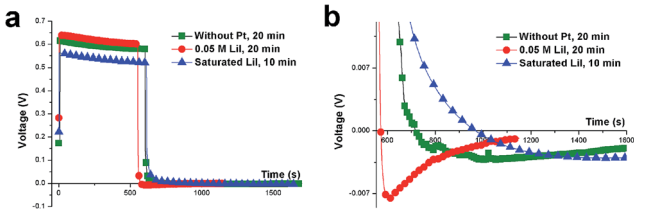

Fig. 7 (a) V_{oc} of PSCs as a function of discharging time. (b) Discharge curves zoomed in.

Fig. 7 shows the measured V_{oc} profile as a function of time during charging and discharging. Three V_{oc} curves decreased slowly under irradiation and sharply turned negative when the light was off. The discharge voltage polarity of each PSC was reversed compared with its photovoltage, indicating that the discharging voltage was from the capacitor section. The V_{oc} values ranged from 0.55–0.62 V. The small difference was related to those variations in catalyst, electrolyte and internal resistance. Fig. 8 shows the photocurrent with respect to charging and discharging duration. Under irradiation, the PSC without Pt catalyst had the lowest current density due to relatively low catalytic effect of CNTs, while the one with saturated LiI in the electrolyte had the highest photocurrent when energy conversion and storage reached a balance. When the light was off, all photocurrent current curves were down to the negative range, which indicates that the $WO_3 \cdot H_2O$/CNTs/PVDF composite on the counter electrode provides the energy storage function. The maximum capacitance observed was 1.98 mC cm^{-2} from the PSC without Pt catalyst, higher than 1.83 mC cm^{-2} with saturated LiI in the electrolyte, 1.38 mC cm^{-2} with the regular electrolyte. It implies that a PSC with higher energy conversion capability usually has lower energy storage. Fig. S2† shows that the energy storage is little related to the charging duration. The electrical impedance spectra as shown in Fig. S3† indicate that the contact between the $WO_3 \cdot H_2O$/CNTs/PVDF composite film and the FTO substrate caused a large resistance, which could potentially be reduced to further improve the performance of PSCs.

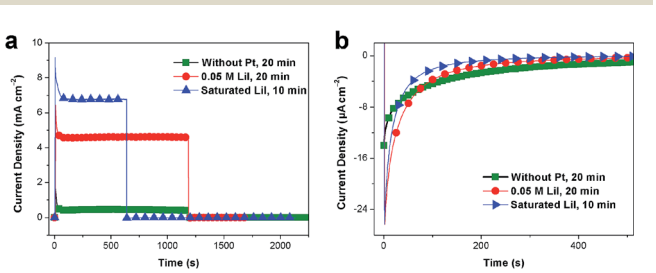

Fig. 8 (a) Charge and discharge *J*–*t* curves of PSCs. (b) Discharge curves zoomed in.

4. Conclusion

We fabricated a two-electrode PSC by introducing a $WO_3 \cdot H_2O$/CNTs/PVDF composite film onto the counter electrode. $WO_3 \cdot H_2O$ nanoplates with high surface area contributed to the energy storage capacity of the PSC. The PSC with regular DSSC electrolyte displays a η of 2.12% with a simultaneous energy storage of 1.38 C cm^{-2}. The highest energy storage (1.98 C cm^{-2}) was observed from a PSC with Pt catalyst on the counter electrode. Higher Li^+ concentration in the electrolyte is helpful to maintain the photocurrent at a larger value during irradiation. As a freestanding flexible composite, $WO_3 \cdot H_2O$/CNTs/PVDF films could be easily loaded onto the counter electrode of DSSCs as the energy storage part, which facilitate the fabrication of PSCs. It is possible to obtain higher performance of PSCs by optimizing the contact between the electron collectors and the pseudocapacitive electrode materials. In addition, the effect of moles of H_2O in tungsten oxide molecule on the performance of PSCs and repeatability of devices will be investigated in the near future.

Acknowledgements

This work was supported by the US National Institute of Health (Grant No. 1DP2OD008678-01). This research utilized NSF supported shared facilities at the University of Wisconsin.

Notes and references

1 D. Schmidt, M. D. Hager and U. S. Schubert, *Adv. Energy Mater.*, 2016, **6**, 1500369.
2 X. Xue, S. Wang, W. Guo, Y. Zhang and Z. Wang, *Nano Lett.*, 2012, **12**, 5048–5054.
3 Z. Zhang, X. Chen, P. Chen, G. Guan, L. Qiu, H. Lin, Z. Yang, W. Bai, Y. Luo and H. Peng, *Adv. Mater.*, 2014, **26**, 466–470.
4 T. N. Murakami, N. Kawashima and T. Miyasaka, *Chem. Commun.*, 2005, 3346–3348.
5 W. Guo, X. Xue, S. Wang, C. Lin and Z. Wang, *Nano Lett.*, 2012, **12**, 2520–2523.
6 M. Yu, W. D. McCulloch, D. R. Beauchamp, Z. Huang, X. Ren and Y. Wu, *J. Am. Chem. Soc.*, 2015, **137**, 8332–8335.
7 T. Miyasaka and T. N. Murakami, *Appl. Phys. Lett.*, 2004, **85**, 3932–3934.
8 J. Xu, Y. Chen and L. Dai, *Nat. Commun.*, 2015, **6**, 1–7.
9 L. Xing, Y. Nie, X. Xue and Y. Zhang, *Nano Energy*, 2014, **10**, 44–52.
10 X. Zhang and H. Jiang, *Appl. Phys. Lett.*, 2015, **106**, 103903.
11 X. Xue, P. Deng, S. Yuan, Y. Nie, B. He, L. Xing and Y. Zhang, *Energy Environ. Sci.*, 2013, **6**, 2615–2620.
12 A. Takshi, H. Yaghoubi, T. Tevi and S. Bakhshi, *J. Power Sources*, 2015, **275**, 621–626.
13 X. Huang, X. Zhang and H. Jiang, *J. Power Sources*, 2014, **248**, 434–438.
14 X. Zhang, X. Huang, C. Li and H. Jiang, *Adv. Mater.*, 2013, **25**, 4093–4096.
15 X. Xiao, T. Ding, L. Yuan, Y. Shen, Q. Zhong, X. Zhang, Y. Cao, B. Hu, T. Zhai, L. Gong, J. Chen, Y. Tong, J. Zhou and Z. L. Wang, *Adv. Energy Mater.*, 2012, **2**, 1328–1332.
16 X. Huang, H. Liu, X. Zhang and H. Jiang, *ACS Appl. Mater. Interfaces*, 2015, **7**, 27845–27852.
17 S. Cong, Y. Tian, Q. Li, Z. Zhao and F. Geng, *Adv. Mater.*, 2014, **26**, 4260–4267.
18 J. Xu, T. Ding, J. Wang, J. Zhang, S. Wang, C. Chen, Y. Fang, Z. Wu, K. Huo and J. Dai, *Electrochim. Acta*, 2015, **174**, 728–734.
19 R. Yuksel, C. Durucana and H. E. Unalana, *J. Alloys Compd.*, 2016, **658**, 183–189.
20 L. Gao, X. Wang, Z. Xie, W. Song, L. Wang, X. Wu, F. Qu, D. Chen and G. Shen, *J. Mater. Chem. A*, 2013, **1**, 7167–7173.
21 Y. Tian, S. Cong, W. Su, H. Chen, Q. Li, F. Geng and Z. Zhao, *Nano Lett.*, 2014, **14**, 2150–2156.
22 Z. Zhang, G. Zhang, L. He, L. Sun, X. Jiang and Z. Yun, *CrystEngComm*, 2014, **16**, 3478–3482.
23 B. Wang, X. Lu, Y. Tang and W. Ben, *ChemElectroChem*, 2016, **3**, 55–65.
24 Y. Zhang, Y. Liu, J. Chen, Q. Guo, T. Wang and H. Pang, *Sci. Rep.*, 2014, **4**, 5687.
25 T. Mei, T. Li, H. Bi, L. Wang, Y. Zhu and Y. Qian, *Eur. J. Inorg. Chem.*, 2010, 4314–4320.
26 Z. Wang, S. Zhou and L. Wu, *Adv. Funct. Mater.*, 2007, **17**, 1790–1794.
27 C. Jo, I. Hwang, J. Lee, C. Lee and S. Yoon, *J. Phys. Chem. C*, 2011, **115**, 11880–11886.
28 J. Ma, L. Zhou, C. Li, J. Yang, T. Meng, H. Zhou, M. Yang, F. Yu and J. Chen, *J. Power Sources*, 2014, **247**, 999–1004.
29 J. R. Jennings and Q. Wang, *J. Phys. Chem. C*, 2010, **114**, 1715–1724.